Cardiac Motion Reconstruction Using LKT Algorithm from 2D and 3D Echocardiography

Alice Gao[1], W. Li[2,3], C. Lin[2], M. Loomes[3], X. Gao[3]

[1] Barts and The London School of Medicine and Dentistry, Queen Mary, University of London, London E1 2AD, UK; a.gao@smd11.qmul.ac.uk
[2] Biomedical Engineering Institute, Fuzhou University, Fuzhou, Fujian 350002, China
[3]School of Science and Technology, Middlesex University, London,NW4 4BT. UK.

Abstract- *The rhythm of the heart endows us with not only a life insurance but also a barometer indicating any potential abnormities. Hence the accurate measurement of heart motion has profound clinical benefit in assisting diagnostic decision making and yet remains a challenging issue to be confronted. Perceptibly, heart motion can be quantified manually from M-mode diagrams of echocardiographs which are created by way of sound waves while a patient undergoing scanning. Alternatively, the motion can be monitored automatically by post-image processing techniques analyzing B-mode video sequences. This paper explores the feasibility of the application of Lucas-Kanada-Tomasi algorithm towards the reconstruction of m-mode diagrams from 2D sequences and tissue velocity curves from 3D video clips for the left ventricle. Preliminary results reveals promising match between the post-processing findings and real-time scanning data and being in consistent agreement with the similar studies.*

Keywords: 2D and 3D echocardiographs, M-mode, B-mode, LKT algorithm, cardiac motion reconstruction

1. Introduction

Echocardiography has become an inseparable addition to the current array of advanced medical equipment, largely due to its competitive nature of being non-invasive, portable, inexpensive and easy to operate, leading to it being a ubiquitous imaging tool. More importantly, echocardiography displays the moving heart in real time, revealing the health status of the heart in vivo. One of the key indicators of potential heart-related diseases including ischemic is the function of heart motion, in which parameters such as directional moving curves, amplitude, velocity, and acceleration all play an important part.

In general, an echocardiography scanner has a built-in motion mode (i.e, m-mode) diagram depicting the moving patterns on a pre-defined line, in addition to the reconstruction of B-mode images (i.e., brightness sequenced images). In this way, an m-mode graph is rendered by using ultrasonic wave beams based on the principles frequency shift, the same way as to produce B-mode video images.

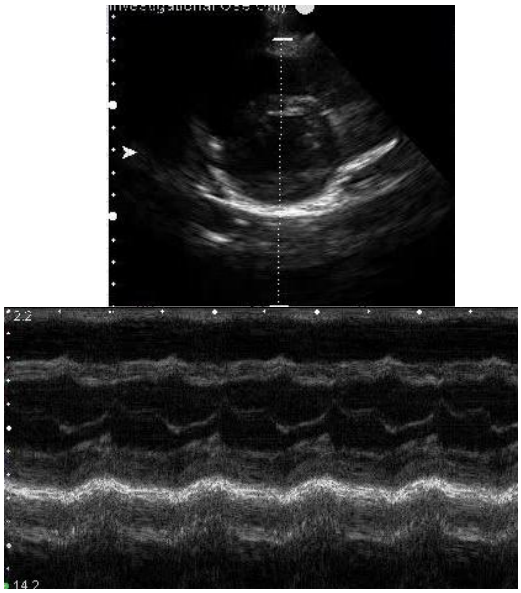

Figure 1. An m-mode diagram (bottom) acquired along the scanning line shown on the top image of left ventricle, which are acquired using Sonix Tablet.

Figure 1 demonstrates an example of m-mode waveform diagram (bottom) and a b-mode image (top) of a 2D echocardiograph. On an m-mode diagram, a

number of measurements can be performed, including left ventricular dimensions (e.g., LVDd, LVDs, PWT, etc..), aortic root and left atrial dimensions (e.g., AO, LA) as well as a number of motion parameters, such as velocity (or slope).

In 3D/4D situations, tissue velocity curves can be constructed in real time, as illustrated in Figure 2. In this case, a tool of Tissue Velocity Imaging (TVI) needs to be in place which applies the principle of myocardial Doppler frequency shifts to quantify myocardial tissues motion (right graph) where the velocity curve refers to the point circled on the top left of the graph.

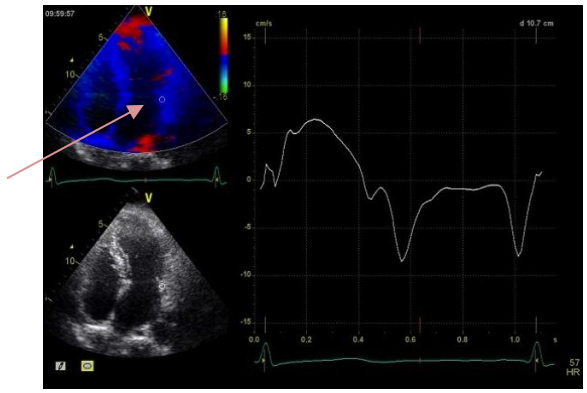

Figure 2. 3D/4D echocardiograph with tissue velocity curve (right) that correlates with the point circled in white on the top-left graph pointed by the arrow. These data are obtained from GE Vivid 7 scanner. The colour blue refers to the blood flow being away from the receiver whilst the red colour towards the transducer.

Ideally, any measurement related to the motion should be performed manually on a scanner in real time to reflect the up to date situation of the heart, which however at present is rarely feasible due to the compelling need of use of the scanner. Furthermore further investigations might be in need at a later stage necessitating the measurements on different direction lines. As a result, post processing on B-mode images have been actively researched in an attempt to re-build motion diagrams. Towards this end, the focus is shifted on to the study of optical flow that reflects velocities by using brightness patterns in an image [1, 2]. Capitalizing from the Lucas-Kanade algorithm, a number of promising optical flow techniques have been developed for evaluation of heart motions together with the verification techniques [3-5]. More recently, motion analysis of the heart has been deepened into biological (tissue) level by investigating myocardial motion [6]. Again, B-mode images constitute the starting point.

Optical flow works on the direct discovery of image motion at each pixel level based on brightness variations from spatio-temporal images. Although the approach can work on dense motion fields, it remains sensitive to the change of appearance resulting from the variations of brightness in images. Therefore it may be more suitable for video sequences with relative small motions.

On the other hand, an ultrasonic image can only generate a fan-shape view window depicting the characteristics of the heart being in a constant motion, suggesting that each image frame may always introduce new points/objects that are not present in the previous frame, leading to a wrong match of brightness-based points to a certain extent.

Furthermore, echocardiography are composed from 2D ultrasonic images that suffers from mixed outlines of gray level intensity and partial area occlusion with blurry edges, therefore the quality of the images are of generally low resolution. As a direct result, searching for the points with similar brightness or intensity values remains a challenge task while applying the optical flow technique, implying feature selections in an automatic way is very difficult. In this study, a slightly different approach is proposed, which classifies the motion patterns first and then tracks the feature points in a class which are defined by the user towards the reconstruction of M-mode diagrams and tissue velocity curves.

The overall aim of this work is to develop a system that circumvents some of the underlying problems inherent in the analysis of the dynamics of the heart by the application of Lucas-Kanade-Tomasi (LKT) motion tracking algorithm [7].

The original idea of the implementation of LKT intends to deal with the problem inherited from traditional image registration that is generally computationally costly. KLT makes efficient consideration of the spatial intensity information to direct the search towards the positions that can generate the best match. It therefore executes faster than traditional techniques by examining far fewer potential matches between the images. In this investigation, each video clip contains up to 2 seconds of duration of the information of a beating heart, arriving at around a hundred 2D frames with an average size of 650 x 400 pixels each, whereas 3D echocardiography is inherently volumetric. Initial feature points are selected manually or segmented on the first frame, which are then tracked using LKT approach on the following frames.

2. Methodology

2.1 Lucas-Kanade-Tomasi(KLT) algorithm

Since the seminal publication of Lucas-Kanade approach [3] on motion study using the optical flow technique, plethora algorithms are on the offer in providing solutions to solve two unknown parameters in one equation. As shown in Eq. (1) where optical flow is expressed from on frame (left) to the next frame (right) with the displacement $\vec{\boldsymbol{d}} = (\xi, \eta)$ occuring at the point (x, y), (ξ, η) are the two unknowns.

$$I(x, y, t) = I(x + \xi, y + \eta, t + \tau) \qquad (1)$$

Based on the Taylor expansion series, the following formula exists.

$$I(x + \xi, y + \eta, t + \tau) \approx I(x, y, t) + \frac{\partial I}{\partial x}\xi + \frac{\partial I}{\partial y}\eta + \frac{\partial I}{\partial t}\tau \qquad (2)$$

which results in

$$\frac{\partial I}{\partial x}V_x + \frac{\partial I}{\partial y}V_y + \frac{\partial I}{\partial t} = 0 \qquad (3)$$

Where V_x, V_y are the x and y components of the velocity or optical flow of *I(x, y, t)* and $\frac{\partial I}{\partial x}, \frac{\partial I}{\partial y}$ and $\frac{\partial I}{\partial t}$ are the derivatives of the image at (x, y, t) in the corresponding directions.

Again Eq. (3) has two unknowns that cannot be solved as such, a number of methods have since developed, which started with the popular Lucas-Kanade method [3]. It assumes that the flow is essentially constant in a local neighbourhood of the pixel under consideration, and that solves the basic optical flow equations for all the pixels in that neighbourhood, by the least squares criterion.

As an implementation, the LKT algorithm [7] considers the time as a brevity of duration. If images *I* and *J* are the two frames of a video clip, Eq.(1) is redefined as Eq. (4) by omitting the time variable.

$$J(\vec{x} + \vec{d}) = I(x + \xi, y + \eta, t + \tau) \quad (4)$$

$$J(\vec{\boldsymbol{x}} + \vec{\boldsymbol{d}}) = I(\vec{\boldsymbol{x}}) + n \qquad (5)$$

where *n* indicates noise. The displacement vector $\vec{\boldsymbol{d}}$ is chosen so as to minimize the residue error defined by the double integral over the given window Ψ shown in Eq.(6).

$$\epsilon = \int_{\Psi}[I(\vec{\boldsymbol{x}}) - J(\vec{\mathbf{x}} + \vec{\mathbf{d}})]^2\psi\, d\vec{\boldsymbol{x}}$$
$$= \int_{\Psi}[I(\vec{\boldsymbol{x}}) - \vec{\boldsymbol{g}} \cdot \vec{\boldsymbol{d}} - J(\vec{\boldsymbol{x}})]^2\psi\, d\vec{\boldsymbol{x}}$$
$$= \int_{\Psi}[h - \vec{\boldsymbol{g}} \cdot \vec{\boldsymbol{d}}]^2\psi\, d\vec{\boldsymbol{x}} \qquad (6)$$

Where ψ is a weighting function that depends on the image intensity pattern, $J(\vec{\boldsymbol{x}} + \vec{\boldsymbol{d}}) = J(\vec{\boldsymbol{x}}) + \vec{\boldsymbol{g}} \cdot \vec{\boldsymbol{d}}$ according to Taylor's series that is truncated to the linear term, $h = I(\vec{\boldsymbol{x}}) - J(\vec{\boldsymbol{x}})$, and image gradient $\vec{\boldsymbol{g}} = (\frac{\partial I}{\partial x}, \frac{\partial I}{\partial y})$.

2.2 Point tracking

Minimising Eq.(6) gives Eq. (7).

$$\frac{d\epsilon}{d\vec{\boldsymbol{d}}} = \int_{\Psi} 2\big(h - \vec{\boldsymbol{g}} \cdot \vec{\boldsymbol{d}}\big)\vec{\boldsymbol{g}}\frac{d\vec{\boldsymbol{d}}}{d\vec{\boldsymbol{x}}}\psi\, d\vec{\boldsymbol{x}}$$
$$= \int_{\Psi} 2\big(h - \vec{\boldsymbol{g}} \cdot \vec{\boldsymbol{d}}\big)\vec{\boldsymbol{g}}\psi\, d\vec{\boldsymbol{d}} = 0 \qquad (7)$$

Since $\big(\vec{\boldsymbol{g}} \cdot \vec{\boldsymbol{d}}\big)\vec{\boldsymbol{g}} = \vec{\boldsymbol{g}} \cdot (\vec{\boldsymbol{g}} \cdot \vec{\boldsymbol{d}})^T = \vec{\boldsymbol{g}} \cdot (\vec{\boldsymbol{g}}^T \cdot \vec{\boldsymbol{d}}^T) = (\vec{\boldsymbol{g}} \cdot \vec{\boldsymbol{g}}^T)\vec{\boldsymbol{d}}^T$, the right hand side of Eq.(7) can be written as Eq.(8),

$$\int_{\Psi} \vec{\boldsymbol{g}}\vec{\boldsymbol{g}}^T\vec{\boldsymbol{d}}\psi\, d\vec{\boldsymbol{d}} = \int_{\Psi} h\vec{\boldsymbol{g}}\psi\, d\vec{\boldsymbol{d}} \qquad (8)$$

Providing $\vec{\boldsymbol{d}}$ remains constant within a window Ψ, Eq.(8) can be further processed as

$$G\vec{\boldsymbol{d}} = \vec{\boldsymbol{e}} \qquad (9)$$

where G maintains as a symmetric 2 x 2 matrix

$$G = \int_{\Psi} \vec{g}\vec{g}^T\psi\, d\vec{\boldsymbol{d}} \qquad (10)$$

and

$$\vec{\boldsymbol{e}} = \int_{\Psi}(I - J)\vec{\boldsymbol{g}}\psi\, d\vec{\boldsymbol{d}} \qquad (11)$$

For every pair of adjacent frames, the matrix *G* can be worked out from one frame, by way of estimating the gradients and computing their second order moments. On the other hand, the vector $\vec{\boldsymbol{e}}$ can be computed from the difference between the two frames, along with the gradient *G*. Therefore the displacement $\vec{\boldsymbol{d}}$ can be solved in Eq. (9), which will lead to the location and thereafter tracking of the point of interest in the subsequent frames.

2.3. The complexity of cardiac motion

The heart has sustained a motion of rhythm that cannot be accounted for linearly. Even without the

consideration of the artifact of respiration motion, the heart itself is in a state of constant contraction/expansion as well as shifting in response to the force generated by the movement of blood flows (e.g., by pumping out). Therefore the overall motion of the heart is a non-rigid body transformation, indicating that the displacement $\vec{\boldsymbol{d}}$ in Eq. (8) does not retain constant when time progresses from t to $t + \tau$. As a direct result, in order to apply the LKT approach, each region has to maintain a motion with a relatively constant $\vec{\boldsymbol{d}}$. Therefore classification of the heart structure should be performed first to ensure that within each class or sub-region, constant movement in a certain direction can be found, for example, aorta or left ventricle. In terms of the left ventricle, Figure 3 schematically illustrates a simplified motion diagram in an ideal situation.

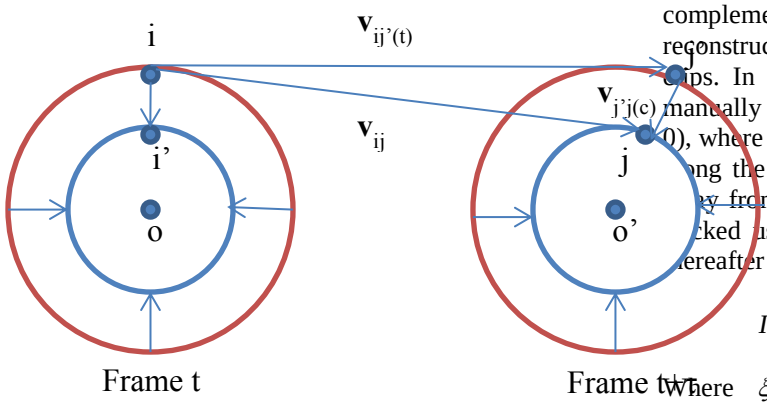

Figure 3. The simulation diagram displaying the ideal situation of left ventricle, where *i is an* arbitrary myocardial point of interest and *j* the corresponding one in the following frame.

For all the feature points in the left ventricle, the motion of the heart is the sum of translation (t) and contraction/expansion as presented in Eq. (12).

$$\vec{\boldsymbol{v}}_{ij} = \vec{\boldsymbol{v}}_{j'j(c)} + \vec{\boldsymbol{v}}_{ij'(t)} \tag{12}$$

$$\iint \vec{\boldsymbol{v}}_{ij} didj = \iint \vec{\boldsymbol{v}}_{j'j(c)}\, didj + \iint \vec{\boldsymbol{v}}_{ij'(t)}\, didj \tag{13}$$

$i.e.,$

$$\iint \vec{\boldsymbol{v}}_{j'j(c)} = \iint (\vec{\boldsymbol{v}}_{j'} - \vec{\boldsymbol{v}}_{j}) = \iint (\vec{\boldsymbol{v}}_{j'} - \vec{\boldsymbol{v}}_{o'}) - \iint (\vec{\boldsymbol{v}}_{j} - \vec{\boldsymbol{v}}_{o'}) = 0 \tag{14}$$

As illustrated in Figure 3, in an ideal situation, the sum of the movement of contraction and expansion with reference to the ventricle centre, $v_{o'}$, for all the tissue points in the left ventricle, falls to zero.

Therefore the overall movement of the left ventricle is

$$\vec{\boldsymbol{v}}_m = \iint \vec{\boldsymbol{v}}_{ij'}\, didj \tag{15}$$

which represents the translation of the heart, i.e., the centre point $\vec{\boldsymbol{o}}$ in the left frame can be treated as shifted $\vec{\boldsymbol{v}}_m \times \tau$ units into $\vec{\boldsymbol{o}}'$ on the following frame. In this way, the remaining contraction/expansion motion $\vec{\boldsymbol{v}}_{j'j(c)}$ can be investigated separately by way of optical flow technique.

2.4 Reconstruction of M-mode diagrams

M-mode diagrams can be applied to analyze the motion patterns along a scanning line, as demonstrated in Figure 1. In a 2D form, the M-mode waveform can only be acquired in real time when the scanning line is defined. Since post image processing is complementary, necessitating the need of reconstruction of m-mode from the acquired video clips. In this study, after a line, $y=a\ x$, is assigned manually passing through the ventricle centre $\vec{\boldsymbol{o}}$ = (0, 0), where a is a constant and the motion direction being along the line (i.e., contracting towards or expanding away from the centre), the points on the line are then tracked using Eq. (9), whereas the m-mode image is thereafter regenerated using Eq.(16) based on Eq. (12).

$$I_{m\text{-}mode}(t+\tau) = I_{i+1}(x + \xi, \boldsymbol{y}) \tag{16}$$

where ξ is the displacement compensating the translation movement expressed in Eq. (12), $\boldsymbol{y}$ representing all the points along the pre-defined line, $y = a\ x$.

2.5 Simulation of velocity curve

Due to the advances of imaging technology, tissue velocity imaging (TVI) tools are available in a number of 3D (= 4D with time) ultrasonic scanners, as illustrated in Figure 2. The speed value in TVI is calculated based on the movement of myocardium towards or away from the scanner transducer. In this investigation, the velocity of any pivot point is simulated using Eq. (17) that are figuratively explained in Figure 4, where v_x and v_y are obtained using Eq. (9), $\theta = atan(y_o/x_o)$, and $\phi = atan(v_y/v_x)$.

$$\vec{\boldsymbol{v}}_l = \sqrt{|v_y|^2 + |v_x|^2} \times \cos(\phi - \theta) \tag{17}$$

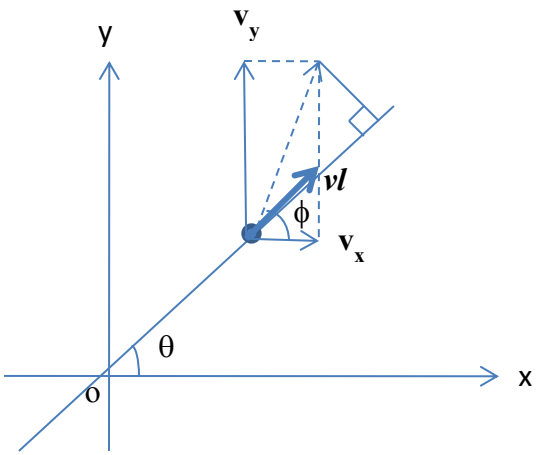

Figure 4. Illustration of the distribution of a velocity along each direction.

3. Results

The simulation is built on the Matlab program of KLT algorithm [9] and an in-house C++ program for motion analysis [8]. Figure 4 illustrates the M-mode regeneration for the image displayed in Figure 1.

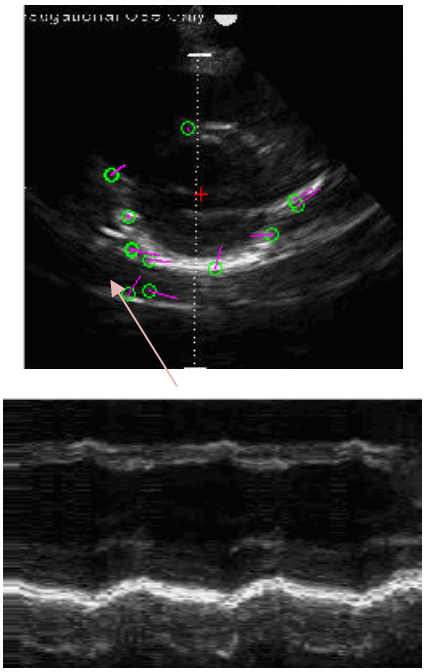

Figure 4. M-mode reconstruction (bottom) for the point near the scanning line as shown by the arrow on the top image, whereas the original m-mode graph is given in Figure 1.

With regard to tissue velocity estimation, Figure 5 demonstrates the re-creation of the velocity curve for the one displayed in Figure 2.

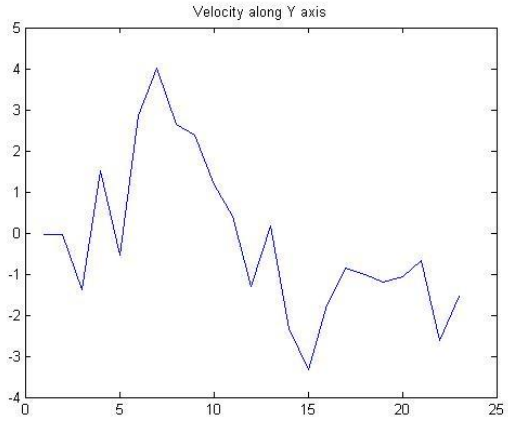

Figure 5. Tissue velocity regeneration using the approach in this study for 3D video image (shown in Figure 2).

Estimating from the appearance of waveform of the velocity in Figure 5, the post-reconstruction to a large extent, bears similarities. After calibration to be in the same unit that was applied while performing in vivo scanning, the measurement of velocity values reveals the average difference between known velocity values (such as shown in Figure 2) and the values obtained from the approach proposed in this study is within 4 pixels, equivalent to 4 mm, which is considered very reasonable [8]. However large scale of quantitative evaluation will be performed in the near future, since there are only ten sets of data are at deposit in this study.

When comparing m-mode waveforms between the original one (Figure 1) and the rendered one (as shown in Figure 4), the challenges lie on the detection of edges from which measuring the first order of derivative (i.e., velocity) of m-mode diagrams can be achieved, as demonstrated in Figure 6. Since the calculations account for the values of edges of m-mode diagrams, variations on edges can contribute to the comparisons, especially, when two images are generated in different ways, one based on the properties of ultrasound and one re-rendered according to the tracking of optical flow. All in all, the differences are within the range of 5 pixels, which again needs to be further exploited in the future.

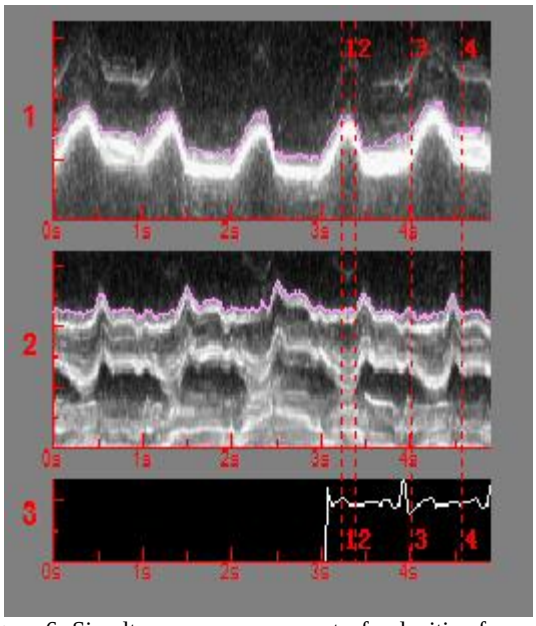

Figure 6. Simultaneous measurement of velocities from m-mode diagrams. Two different scanning lines from the same ventricle are illustrated here.

4. Discussion and Conclusion

Because of the convoluted nature of the heart motion, the application of existing popular motion detection methods remains far from a plug-in process, implying each sub-structure of the heart has to be dealt with individually, by taking into consideration of its specific characteristics.

With this in mind, the motion status of the left ventricle has been investigated in details in this study from both 2D and 3D video sequences and from both short axis (Figure 1) and long axis (Figure 2) parasternal views. Initial evaluation results have shown a very good match in the generation of M-mode diagrams and velocity curves. In 2D form where velocity data are not available, the motion curves can then be built on by using the first derivative of the edge of the M-mode images as illustrated in Figure 7, which can lead subsequent analysis of dynamics of the heart.

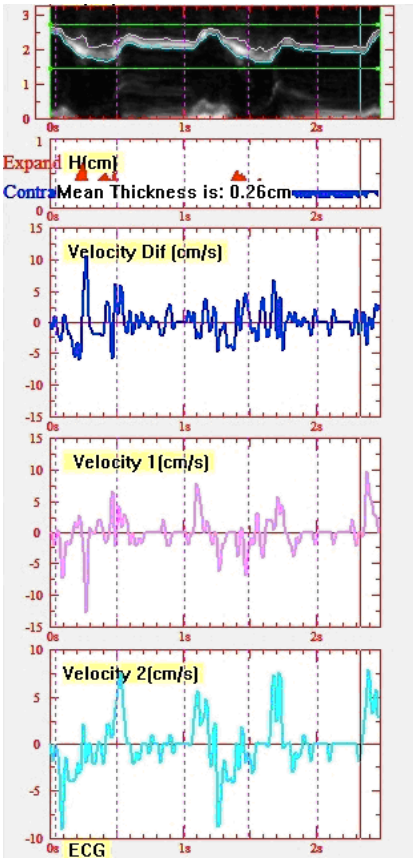

Figure 7. Velocity analysis from m-mode diagrams.

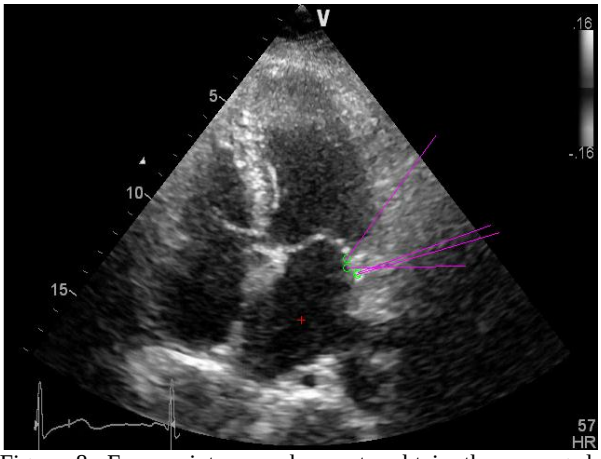

Figure 8. Four points are chosen to obtain the averaged velocity curve shown in Figure 5. The mark '+' indicates the ventricle centre.

With respect to the simulation of velocity curves from 3D video sequences, the evaluation tends to be a straightforward process providing the exact direction of the transducer is known. As it happens, the direction of the velocity shown in Figure 2 is always along the

transducer, i.e, showing the colour blue while away from the transducer beams and red while towards them. Therefore averaged velocity is given in Figure 5 from the four neighbouring points as presented in Figure 8 to compensate the variations induced by the change of the position of the transducer.

Future work includes to further the evaluation of the proposed implementation of the simulation and improve the accuracy of the point tracking by using KLT algorithm combining both optical flow principles and ultrasonic characteristics.

Acknowledgement

This work forms part of WIDTH project that is funded by the European Commission. Their financial contribution is gratefully acknowledged. Thanks also go to one of the WIDTH partners, Dr. Lianyi Wang, for her medical images and expertise on the subject.

5. References

[1] P. Baraldi, A. Sarti, C. Lamberti, A. Prandini, and F. Sgallari, Evaluation of differential optical flow techniques on synthesized echo images, *IEEE Trans. Biomed. Eng.*, 1996, 43(3), pp. 259–272.

[2] D. Boukerroui, J.A. Noble, M. Brady, Velocity estimation in ultrasound images: a block matching approach, Inf Process Med Imagig. 2003 Jul;18:586-98.

[3] B. D. Lucas, and T. Kanade. "An Iterative Image Registration Technique with an Application to Stereo Vision", *International Joint Conference on Artificial Intelligence*, 1981, pp. 674-679.

[4] D. Sun, S. Roth, and M.J. Black, "Secrets of Optical Flow Estimation and Their Principles", 2010, IEEE Int. Conf. on Comp. Vision & Pattern Recognition.

[5] B. Horn and B. Schunk, "Determining optical flow", *Artif. Intell.*, 1981, 17, pp.185–203.

[6] M. Sühling , M. Arigovindan, C. Jansen , P. Hunziker, and M. Unser, Myocardial motion analysis from B-mode echocardiograms., *IEEE Trans Image Process*, 2005, 14(4), pp.525-36.

[7] J. Shi and C. Tomasi, "Good Features to Track", IEEE *Conference on Computer Vision and Pattern Recognition*,1994, pp. 593-600.

[8] Q. Lin, W. Wu, L. Huang, Y. Lin, "An omnidirectional M-mode echocardiography system and its clinical application", *Computerized Medical Imaging and Graphics*, 2006, 30, pp. 333–338.

[9] http://www.ces.clemson.edu/~stb/klt/, received on January 30, 2013.